Arch Appl Mech (2013) 83:25–42
DOI 10.1007/s00419-012-0630-8

ORIGINAL

**Siavash Kazemirad · Mergen H. Ghayesh · Marco Amabili**

# Thermo-mechanical nonlinear dynamics of a buckled axially moving beam

Received: 17 January 2012 / Accepted: 3 March 2012 / Published online: 22 March 2012


**Abstract** The thermo-mechanical nonlinear dynamics of a buckled axially moving beam is numerically investigated, with special consideration to the case with a three-to-one internal resonance between the first two modes. The equation of motion of the system traveling at a constant axial speed is obtained using Hamilton's principle. A closed form solution is developed for the post-buckling configuration for the system with an axial speed beyond the first instability. The equation of motion over the buckled state is obtained for the forced system. The equation is reduced into a set of nonlinear ordinary differential equations via the Galerkin method. This set is solved using the pseudo-arclength continuation technique to examine the frequency response curves and direct-time integration to construct bifurcation diagrams of Poincaré maps. The vibration characteristics of the system at points of interest in the parameter space are presented in the form of time histories, phase-plane portraits, and Poincaré sections.

**Keywords** Axially moving beams · Post-buckling analysis · Divergence · Nonlinear dynamics · Stability ·

## 1 Introduction

Axially moving systems [1–5] are common constituent elements in mechanical, civil, industrial, and aerospace systems such as in paper sheet processes, textile fibers, band saw blades, conveyor belts, magnetic tapes, robot arms, automobile and aerospace structures, aerial cable tramways, and fluid-conveying pipes.

Physically, as a conservative axially moving system reaches the so-called *critical speed*, one of the natural frequencies of the system, usually the first one, vanishes and the system buckles. Here, it is assumed that the beam reaches the critical axial speed and buckles, and then, the resonant response due to a distributed transverse force about the buckled state as well as complex global dynamics is numerically examined.

Temperature fields develop thermal strains due to thermal expansion or contraction, affecting the dynamical behavior of mechanical systems by producing thermal stresses [6–12]. Therefore, in this paper, thermal loadings, due to a uniform temperature rise, on the beam are included in the model and thus in the equation of motion.

The dynamics of axially moving (and accelerating) beams and strings has received considerable attention in literature [13]. The early nonlinear models of the system started appearing by Mote [14], Thurman and Mote [3], and Shih [4]. These early studies on the nonlinear dynamics of the system were pursued later, for example, by Pakdemirli et al. [15–21], who examined the system dynamics via some analytical techniques such as the method of multiple timescales and matched asymptotic expansion technique. Chen et al. [22–28] extended the previous works by considering several beam models and employing different techniques such as the method of multiple timescales, Galerkin's method, and a finite difference scheme. Several energy dissipation mechanisms

S. Kazemirad · M. H. Ghayesh (✉) · M. Amabili
Department of Mechanical Engineering, McGill University, Montreal, QC H3A 2K6, Canada
E-mail: mergen.hajghayesh@mail.mcgill.ca
Tel.: +1-514-3986290

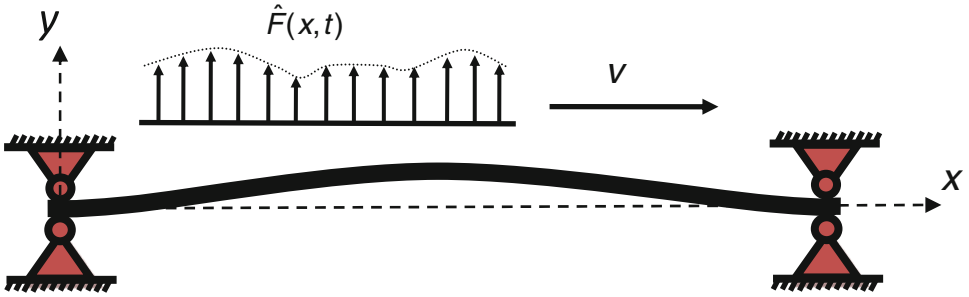


**Fig. 1** Schematic representation of an axially moving beam subject to a uniform temperature rise

were introduced to the system model by Marynowski et al. [29–31]. Further investigations in this area were conducted by Suweken et al. [32–34], Sze et al. [35] and Huang et al. [36], Stylianou and Tabarrok [37], Riedel and Tan [38], and other authors [39–41]. Recently, in a series of paper by Ghayesh et al. [42–58], a systematic research was conducted for linear, nonlinear, internally damped, parametrically excited, and Timoshenko and laminated beam models.

In this paper, the equations for the longitudinal and transverse motions of an axially moving beam subject to a thermal loading are developed via Hamilton's principle. Neglecting the fast dynamics in the longitudinal direction, these two partial differential equations are reduced into an integro-partial differential equation governing the transverse motion of the beam. A closed- form solution for the buckled state and critical speed of the beam is obtained, and the equation of motion over the buckled state is developed. It is assumed that a distributed harmonic load is then applied on the buckled system. The equation is discretized via the Galerkin method and solved using the pseudo-arclength continuation technique along with direct-time integration. The resonant responses of the system including the case with an internal resonance as well as bifurcation diagrams of the system are examined.

## 2 Model development and methods of solution

Figure 1 shows an axially moving beam of length $L$, with constant density $\rho$, axial stiffness $EA$, and flexural rigidity $EI$ traveling at a constant axial speed $v$. Furthermore, the beam is subjected to a pretension $p$, distributed transverse force $\hat{F}(x,t) = \hat{F}(x)\cos(\omega t)$ per unit length along the entire span, and a uniform temperature rise of $\Delta T$.

The equations of motion are derived under the following assumptions: (i) only the planar displacements are considered; (ii) the beam has a uniform cross-sectional area; (iii) rotary inertia and shear deformation are neglected; (iv) the geometric nonlinearity due to the nonlinear relation between the strain and displacement fields is considered; (v) the strains are small even though the displacements can be large (i.e. linear elasticity is applied); (vi) the maximum order of magnitude considered is three; (vii) the external distributed force is assumed to be applied in the transverse direction; (viii) the beam is simply supported; (ix) it is assumed that the external excitation load is applied when the beam is traveling with an axial speed beyond the first critical one; (x) the temperature rise is assumed to be uniform; (xi) it is assumed that the external force is applied after the beam has lost stability in the first mode.

The variation of the potential energy of the beam, after satisfying the hinged-hinged boundary conditions, can be expressed as follows:

$$\int_{t_1}^{t_2} \delta\pi \, \mathrm{d}t = EI \int_{t_1}^{t_2}\int_{0}^{L} \frac{\partial^4 w}{\partial x^4}\delta w \, \mathrm{d}x \, \mathrm{d}t$$
$$-A\int_{t_1}^{t_2}\int_{0}^{L} \frac{\partial}{\partial x}\left[\frac{\partial w}{\partial x}\left(E\left(\frac{\partial u}{\partial x}+\frac{1}{2}\left(\frac{\partial w}{\partial x}\right)^2\right)-\gamma\right)\right]\delta w \, \mathrm{d}x \, \mathrm{d}t$$

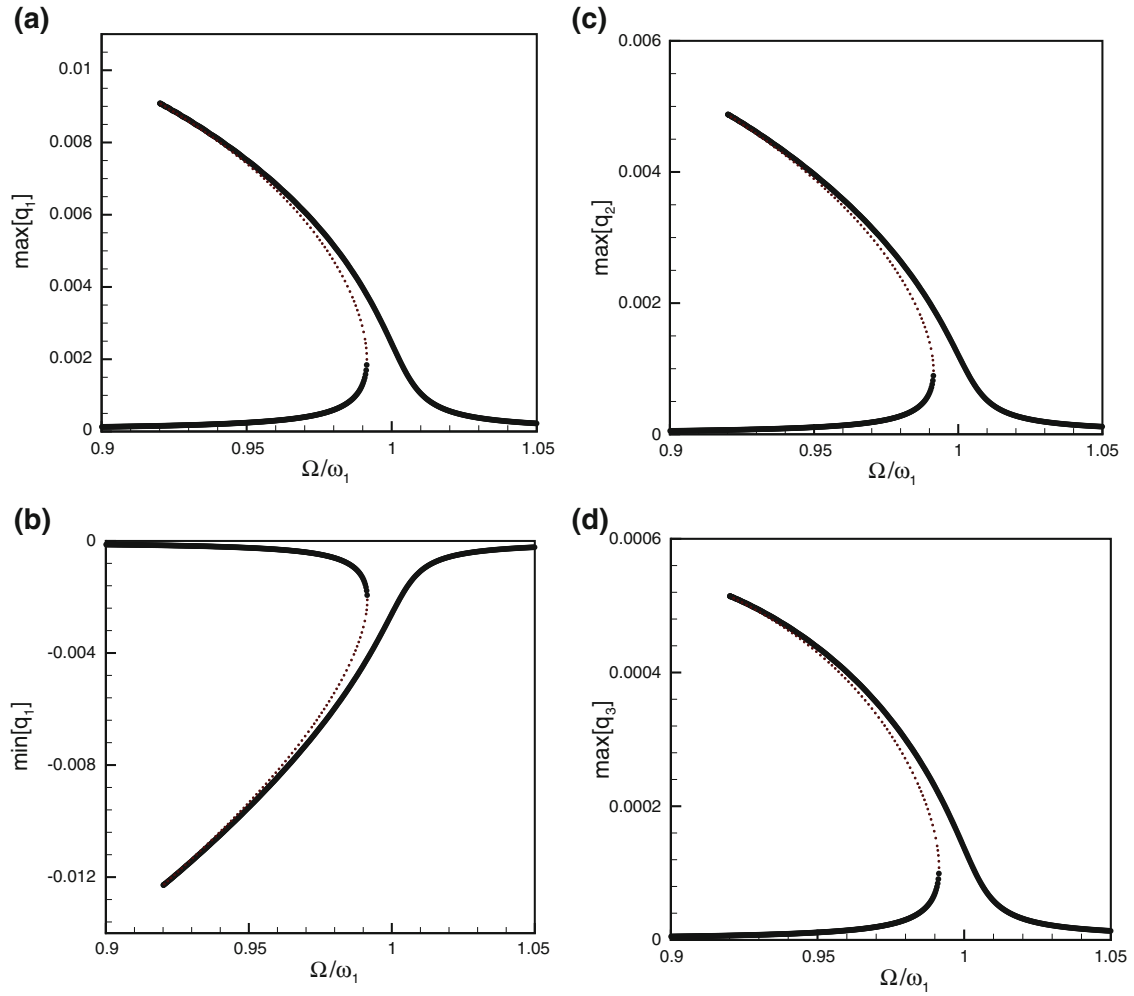


**Fig. 2** The frequency response curve of the system with no internal resonances between the first two modes. **a**, **b** The maximum and minimum of the first generalized coordinate, respectively; **c**, **d** the maximum of the second and third generalized coordinates, respectively. *Bold lines* and *dotted lines* represent the stable and unstable solutions, respectively; $c = 4.5$, $v_1 = 60$, $v_f = 0.8$, $\mu = 0.05$, $\gamma_T = 0.1$, and $f_1 = 0.007$

$$-p\int_{t_1}^{t_2}\int_{0}^{L}\frac{\partial^2 w}{\partial x^2}\delta w\,\mathrm{d}x\,\mathrm{d}t$$
$$-A\int_{t_1}^{t_2}\int_{0}^{L}\frac{\partial}{\partial x}\left(E\left(\frac{\partial u}{\partial x}+\frac{1}{2}\left(\frac{\partial w}{\partial x}\right)^2\right)-\gamma\right)\delta u\,\mathrm{d}x\,\mathrm{d}t, \tag{1}$$

where $\pi$ represents the potential energy, $\gamma = E\,\alpha\,\Delta T$, where $\alpha$ is the thermal expansion coefficient of the beam, and $u(x,t)$ and $w(x,t)$ represent the longitudinal and transverse displacements of the mid-plane of the beam.

The variation of the kinetic energy of the system, after satisfying the hinged-hinged boundary conditions, is given by

$$\int_{t_1}^{t_2}\delta T\,\mathrm{d}t = -\rho A\int_{t_1}^{t_2}\int_{0}^{L}\left(\frac{\partial^2 w}{\partial t^2}+v\frac{\partial^2 w}{\partial x\partial t}\right)\delta w\,\mathrm{d}x\,\mathrm{d}t$$

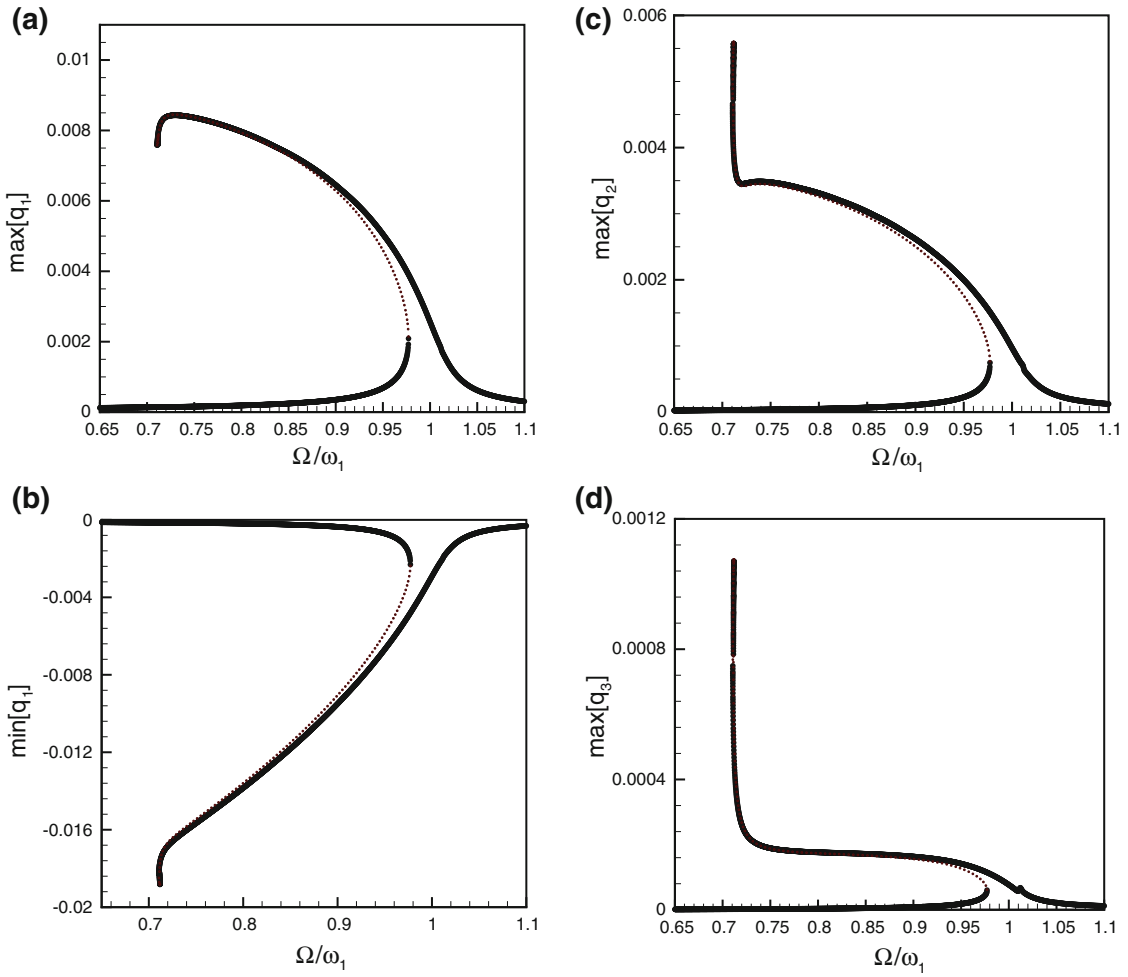


**Fig. 3** The frequency response curve of the system with a three-to-one internal resonance between the first two modes. **a**, **b** The maximum and minimum of the first generalized coordinate, respectively; **c**, **d** the maximum of the second and third generalized coordinates, respectively. *Bold lines* and *dotted lines* represent the stable and unstable solutions, respectively; $c = 3.06$, $v_1 = 60$, $v_f = 0.6$, $\mu = 0.04$, $\gamma_T = 0.1$, and $f_1 = 0.007$

$$
\begin{aligned}
&-\rho A \int_{t_1}^{t_2}\int_{0}^{L} v\left(\frac{\partial^2 w}{\partial x \partial t} + v\frac{\partial^2 w}{\partial x^2}\right)\delta w \,\mathrm{d}x\,\mathrm{d}t \\
&-\rho A \int_{t_1}^{t_2}\int_{0}^{L} \left(\frac{\partial^2 u}{\partial t^2} + v\frac{\partial^2 u}{\partial x \partial t}\right)\delta u \,\mathrm{d}x\,\mathrm{d}t \\
&-\rho A \int_{t_1}^{t_2}\int_{0}^{L} v\left(\frac{\partial^2 u}{\partial x \partial t} + v\frac{\partial^2 u}{\partial x^2}\right)\delta u \,\mathrm{d}x\,\mathrm{d}t. \qquad (2)
\end{aligned}
$$

The variation of the work due to the external distributed force on the beam is given by

$$
\delta W_F = \int_0^L \hat{F}(x)\cos(\omega t)\delta w \mathrm{d}x. \qquad (3)
$$

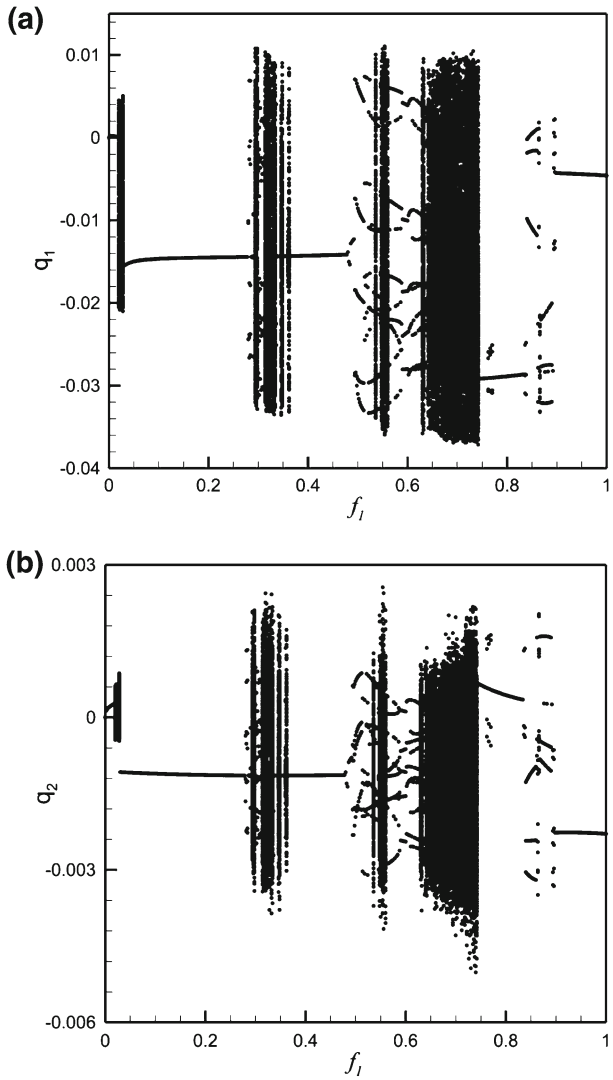


**Fig. 4** Bifurcation diagrams of Poincaré points for increasing forcing amplitude on the system with $\gamma_T = 0.5$, $c = 2.8$, $v_1 = 80$, $v_f = 0.8$, and $\mu = 0.05$; **a** the first mode, and **b** the second mode

Inserting Eqs. (1–3) into Hamilton's principle results in the following equations of motion in the longitudinal and transverse directions:

$$\rho A\left(\frac{\partial^2 u}{\partial t^2}+2v\frac{\partial^2 u}{\partial x\partial t}+v^2\frac{\partial^2 u}{\partial x^2}\right)-A\frac{\partial}{\partial x}\left[E\left(\frac{\partial u}{\partial x}+\frac{1}{2}\left(\frac{\partial w}{\partial x}\right)^2\right)-\gamma\right]=0, \tag{4}$$

$$\begin{aligned}&\rho A\left(\frac{\partial^2 w}{\partial t^2}+2v\frac{\partial^2 w}{\partial x\partial t}+v^2\frac{\partial^2 w}{\partial x^2}\right)+EI\frac{\partial^4 w}{\partial x^4}\\&-A\frac{\partial}{\partial x}\left\{\frac{\partial w}{\partial x}\left[E\left(\frac{\partial u}{\partial x}+\frac{1}{2}\left(\frac{\partial w}{\partial x}\right)^2\right)-\gamma\right]\right\}\\&-p\frac{\partial^2 w}{\partial x^2}-\hat{F}(x)\cos(\omega t)=0,\end{aligned} \tag{5}$$

with the boundary conditions for a hinged-hinged beam as

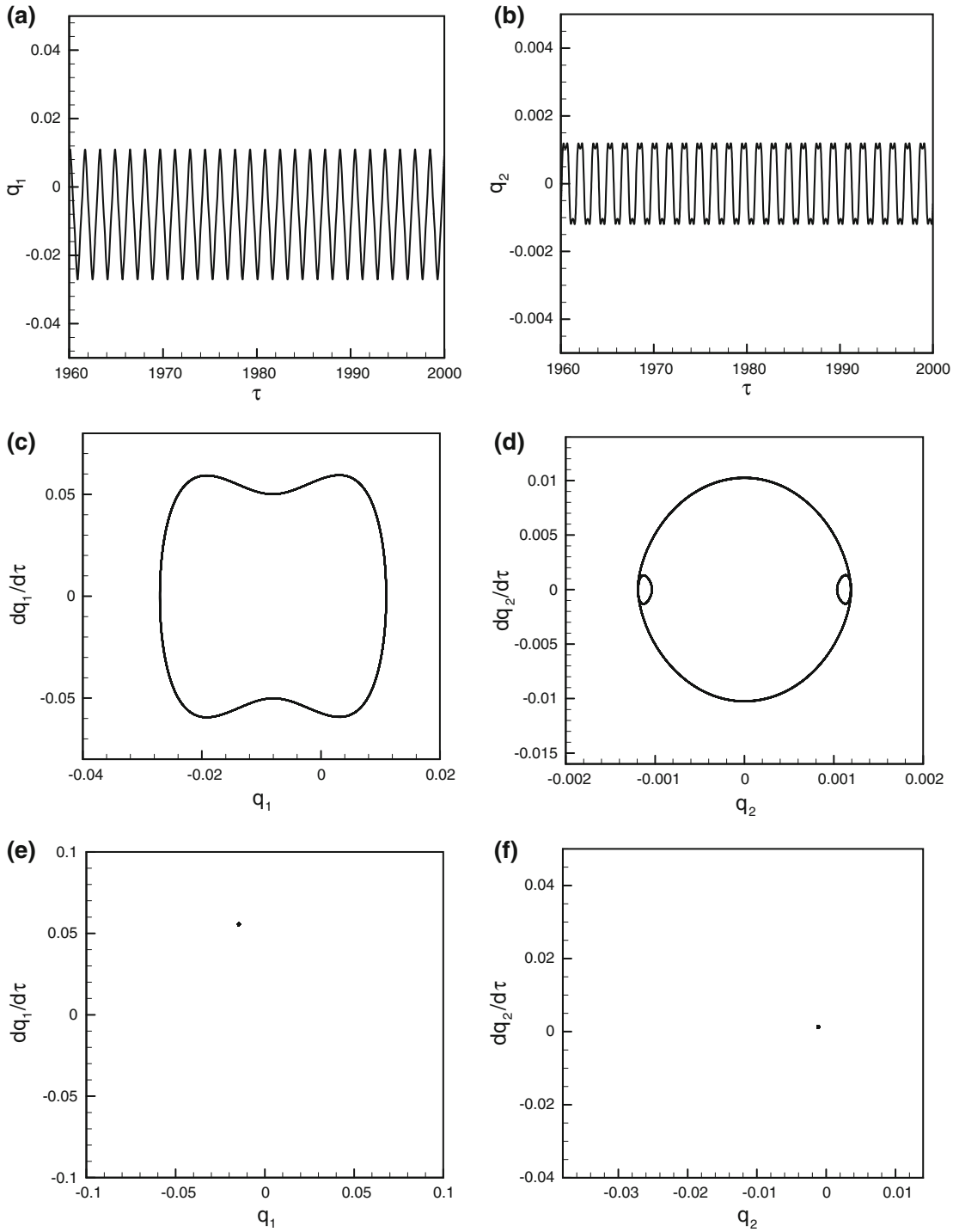


**Fig. 5** Periodic oscillation for the system of Fig. 4 at $f_1 = 0.15$; **a**, **b** time traces of the $q_1$ and $q_2$ motions, respectively; **c**, **d** phase-plane diagrams of the $q_1$ and $q_2$ motions, respectively; **e**, **f** Poincaré sections of the $q_1$ and $q_2$ motions, respectively

$$u|_{x=0} = u|_{x=L} = 0, \tag{6}$$

$$w|_{x=0} = \left.\frac{\partial^2 w}{\partial x^2}\right|_{x=0} = 0,\ w|_{x=L} = \left.\frac{\partial^2 w}{\partial x^2}\right|_{x=L} = 0. \tag{7}$$

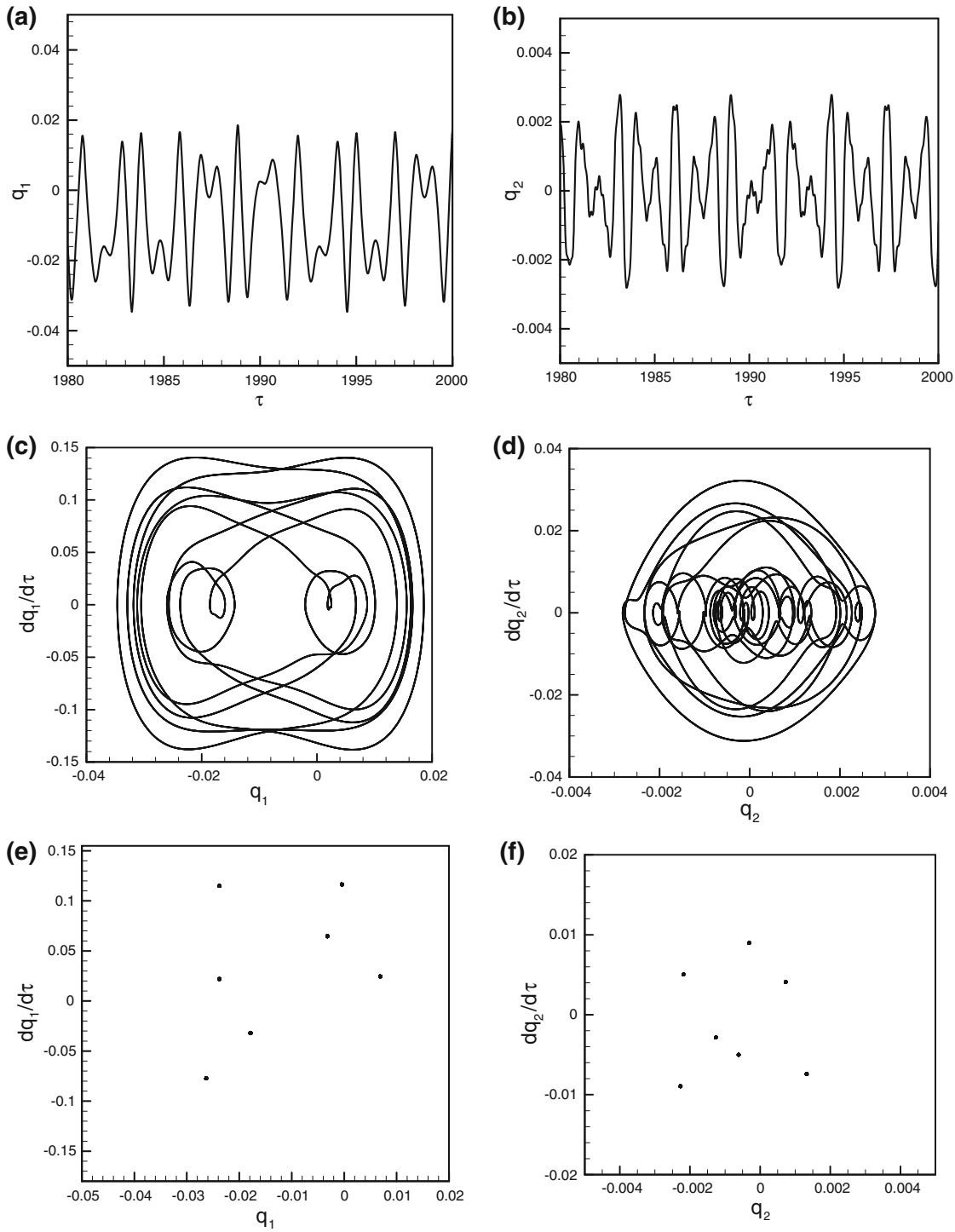


**Fig. 6** Period-7 oscillation for the system of Fig. 4 at $f_1 = 0.284$; **a**, **b** time traces of the $q_1$ and $q_2$ motions, respectively; **c**, **d** phase-plane diagrams of the $q_1$ and $q_2$ motions, respectively; **e**, **f** Poincaré sections of the $q_1$ and $q_2$ motions, respectively

Neglecting the acceleration in the longitudinal direction in Eq. (4) (see [59]) gives an expression of the longitudinal displacement as a function of the transverse one. Substituting this into Eq. (5) gives the following equation for the transverse motion of the beam:

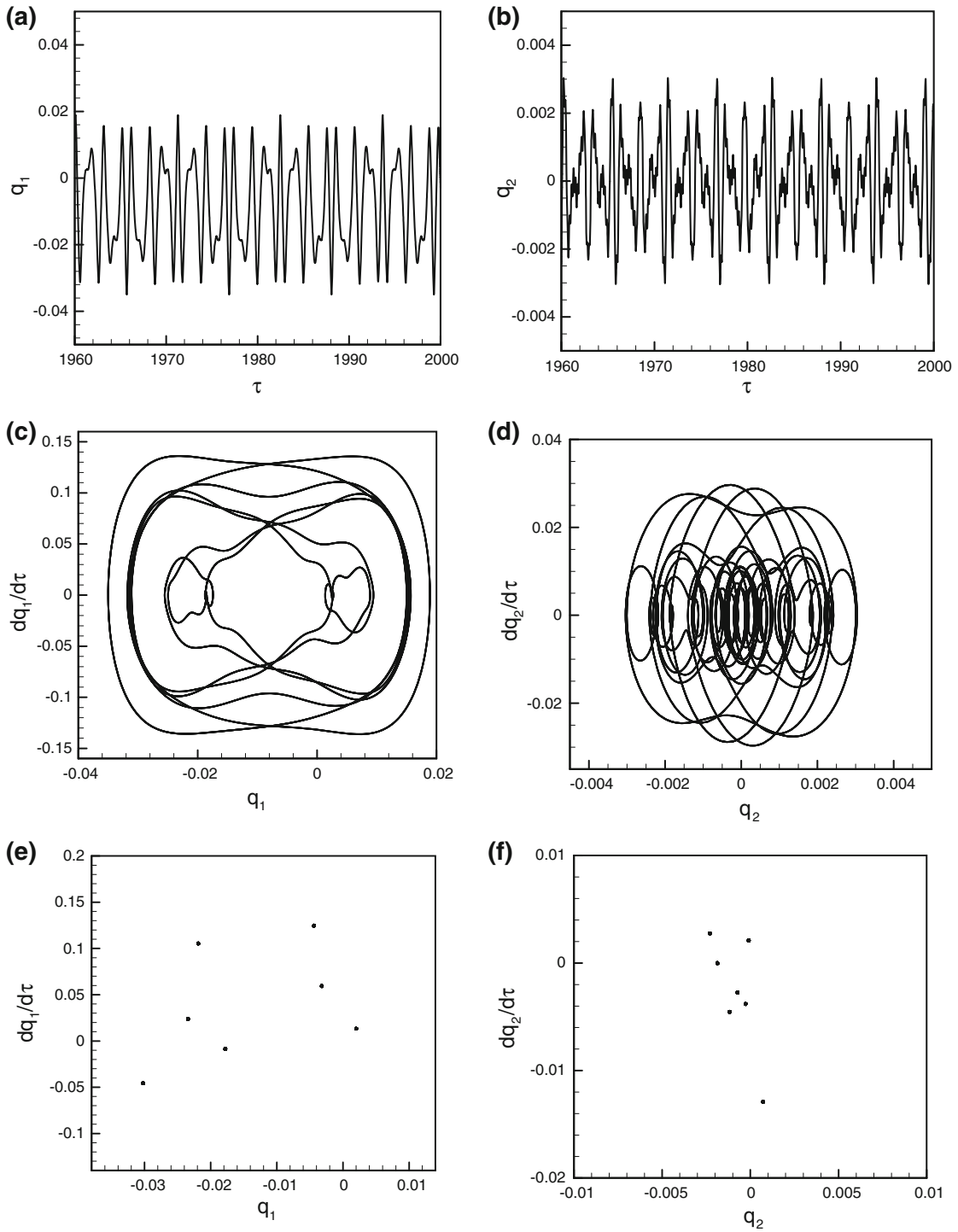


**Fig. 7** Period-7 oscillation for the system of Fig. 4 at $f_1 = 0.310$; **a**, **b** time traces of the $q_1$ and $q_2$ motions, respectively; **c**, **d** phase-plane diagrams of the $q_1$ and $q_2$ motions, respectively; **e**, **f** Poincaré sections of the $q_1$ and $q_2$ motions, respectively

$$EI\frac{\partial^4 w}{\partial x^4} + \rho A\left(\frac{\partial^2 w}{\partial t^2} + 2v\frac{\partial^2 w}{\partial x \partial t} + v^2\frac{\partial^2 w}{\partial x^2}\right) - p\frac{\partial^2 w}{\partial x^2} + A\gamma\frac{\partial^2 w}{\partial x^2}$$
$$= \frac{EA}{2L}\frac{\partial^2 w}{\partial x^2}\int_0^L \left(\frac{\partial w}{\partial x}\right)^2 \mathrm{d}x + \hat{F}(x)\cos(\omega t). \tag{8}$$

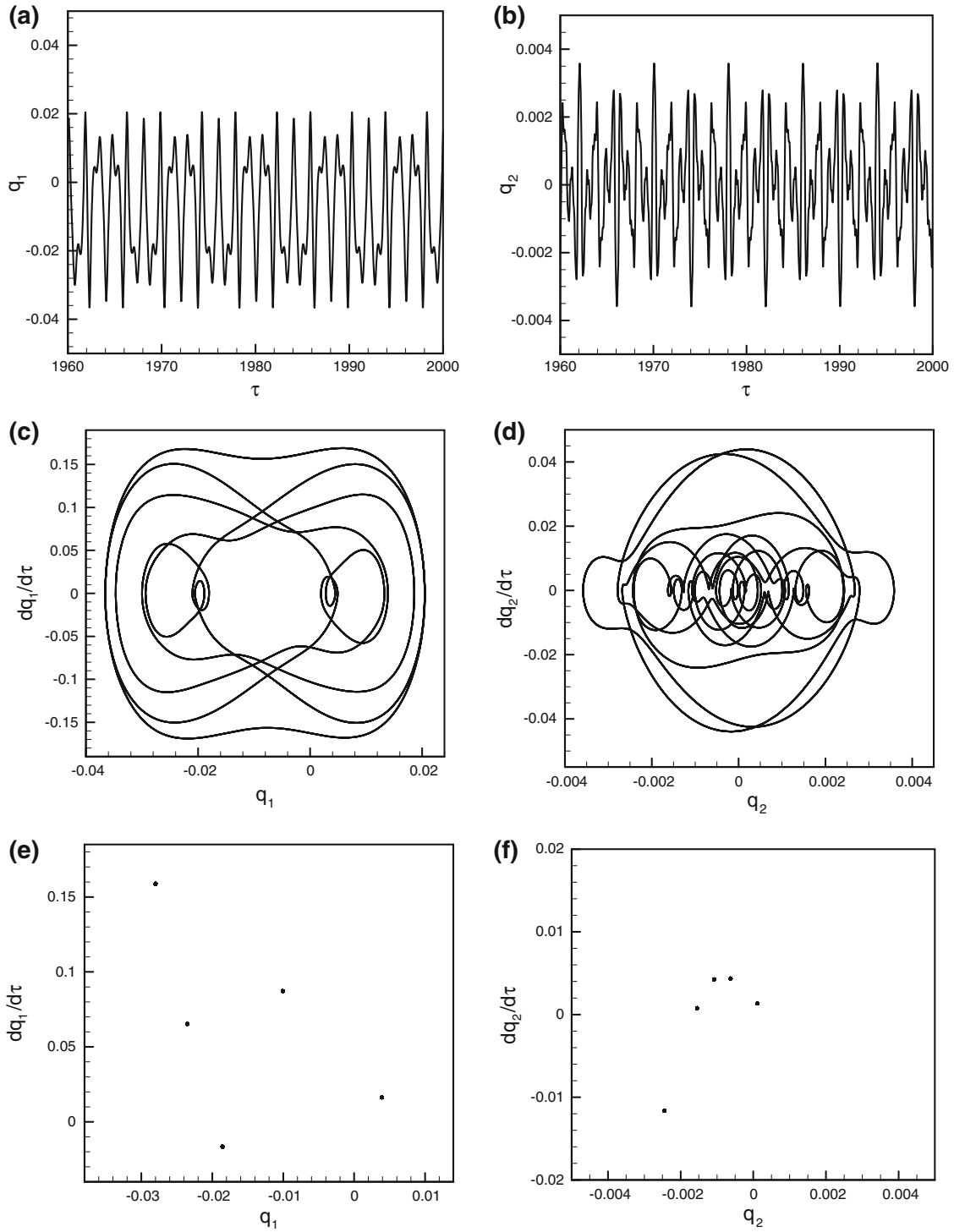


**Fig. 8** Period-5 oscillation for the system of Fig. 4 at $f_1 = 0.600$; **a**, **b** time traces of the $q_1$ and $q_2$ motions, respectively; **c**, **d** phase-plane diagrams of the $q_1$ and $q_2$ motions, respectively; **e**, **f** Poincaré sections of the $q_1$ and $q_2$ motions, respectively

Equation (8) can be rewritten as

$$\frac{\partial^2 \eta}{\partial \tau^2} + 2c\frac{\partial^2 \eta}{\partial \xi \partial \tau} + (c^2 - 1)\frac{\partial^2 \eta}{\partial \xi^2} + v_f^2 \frac{\partial^4 \eta}{\partial \xi^4} + \gamma_T \frac{\partial^2 \eta}{\partial \xi^2}$$

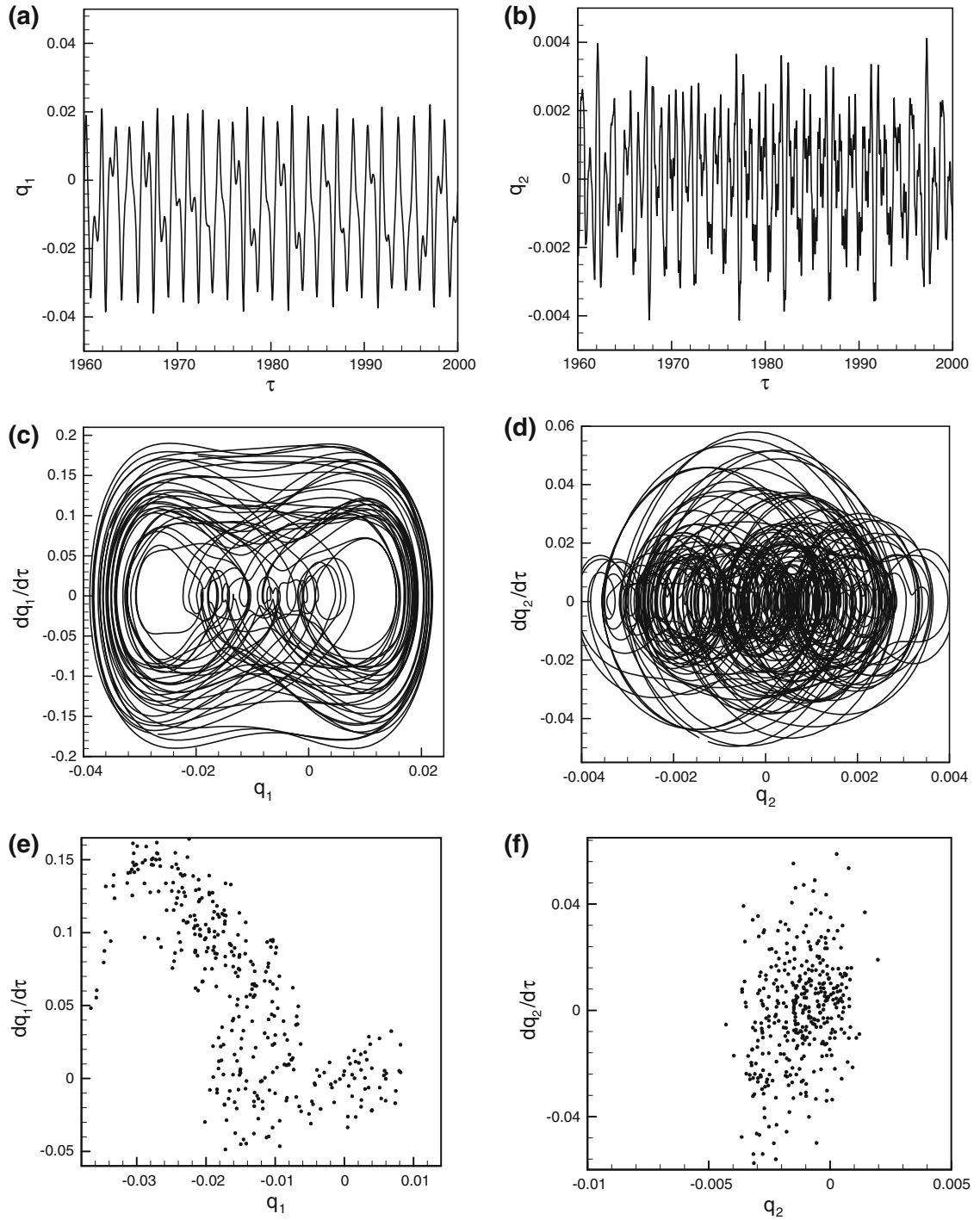


**Fig. 9** Chaotic oscillation for the system of Fig. 4 at $f_1 = 0.700$; **a**, **b** time traces of the $q_1$ and $q_2$ motions, respectively; **c**, **d** phase-plane diagrams of the $q_1$ and $q_2$ motions, respectively; **e**, **f** Poincaré sections of the $q_1$ and $q_2$ motions, respectively

$$= \frac{1}{2} v_1^2 \frac{\partial^2 \eta}{\partial \xi^2} \int_0^1 \left( \frac{\partial \eta}{\partial \xi} \right)^2 \mathrm{d}\xi + F(\xi) \cos(\Omega \tau). \tag{9}$$

with the following change of variables:

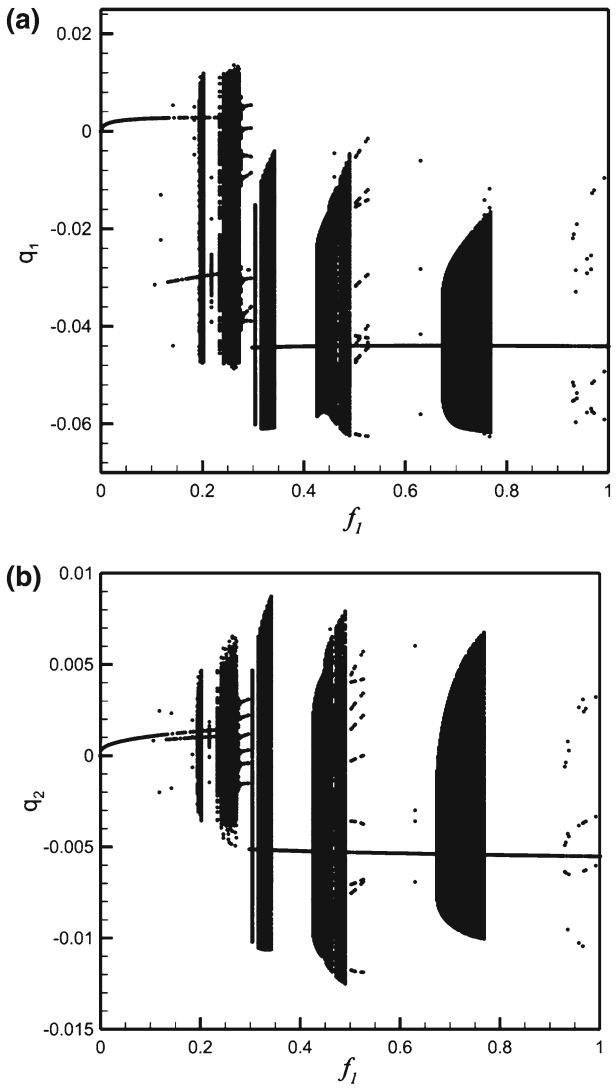


**Fig. 10** Bifurcation diagrams of Poincaré points for increasing forcing amplitude on the system with $\gamma_T = 0.5, c = 3.5, v_1 = 80$, $v_f = 0.8$, and $\mu = 0.05$; **a** the first mode, and **b** the second mode

$$\eta = \frac{w}{L}, \quad \xi = \frac{x}{L}, \; \tau = t\sqrt{\frac{p}{\rho A L^2}}, \; c = v\sqrt{\frac{\rho A}{p}}, \quad v_f = \sqrt{\frac{EI}{pL^2}},$$
$$\gamma_T = \frac{A\gamma}{p}, \; v_1 = \sqrt{\frac{EA}{p}}, \; F = \frac{\hat{F}L}{p}, \; \Omega = \omega\sqrt{\frac{\rho A L^2}{p}}. \tag{10}$$

As is well known, the free system loses stability via divergence at a sufficiently large axial speed, known as the *critical speed*. At this speed, the trivial equilibrium solution bifurcates into two nontrivial equilibrium branches. Setting time derivative of the displacement field equal to zero and solving the resulting spatial-variable-dependent ordinary differential equation results in the following critical speed and nontrivial equilibrium branches in different modes:

$$c_{(k)} = \sqrt{1 + (k\pi v_f)^2 - \gamma_T}, \tag{11}$$
$$\psi_{(k)}(\xi) = \pm\frac{2}{k\pi v_1}\sqrt{c^2 - c_{(k)}^2}\sin(k\pi\xi), \tag{12}$$

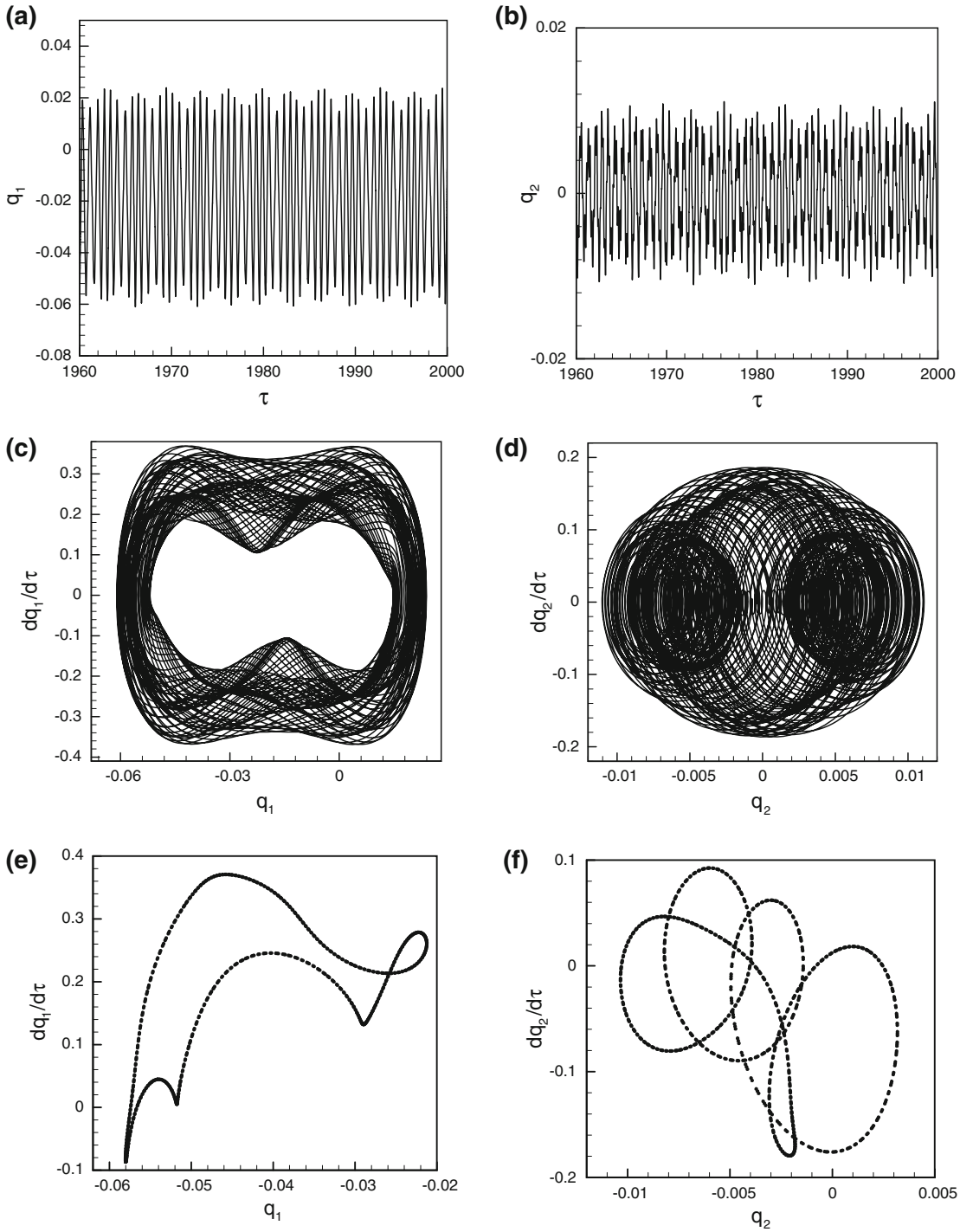


**Fig. 11** Quasiperiodic oscillation for the system of Fig. 10 at $f_1 = 0.43$; **a**, **b** time traces of the $q_1$ and $q_2$ motions, respectively; **c**, **d** phase-plane diagrams of the $q_1$ and $q_2$ motions, respectively; **e**, **f** Poincaré sections of the $q_1$ and $q_2$ motions, respectively

where $k = 1, 2, 3, \ldots$, determines the number of the mode. Positive $\psi_{(k)}(\xi)$ along with the first-mode divergence (i.e. $k = 1$) is considered in the analysis. From physical perspective, since higher order bifurcations need more energy to be activated, the stability is assumed to be lost in the first mode and the system does not reach the second critical speed. Substitution of the new equilibrium solution branches into Eq. (9) using $\eta(\xi, \tau) \rightarrow \psi_{(k)}(\xi) + \eta(\xi, \tau)$ gives the following equation governing the transverse displacement about the buckled state:

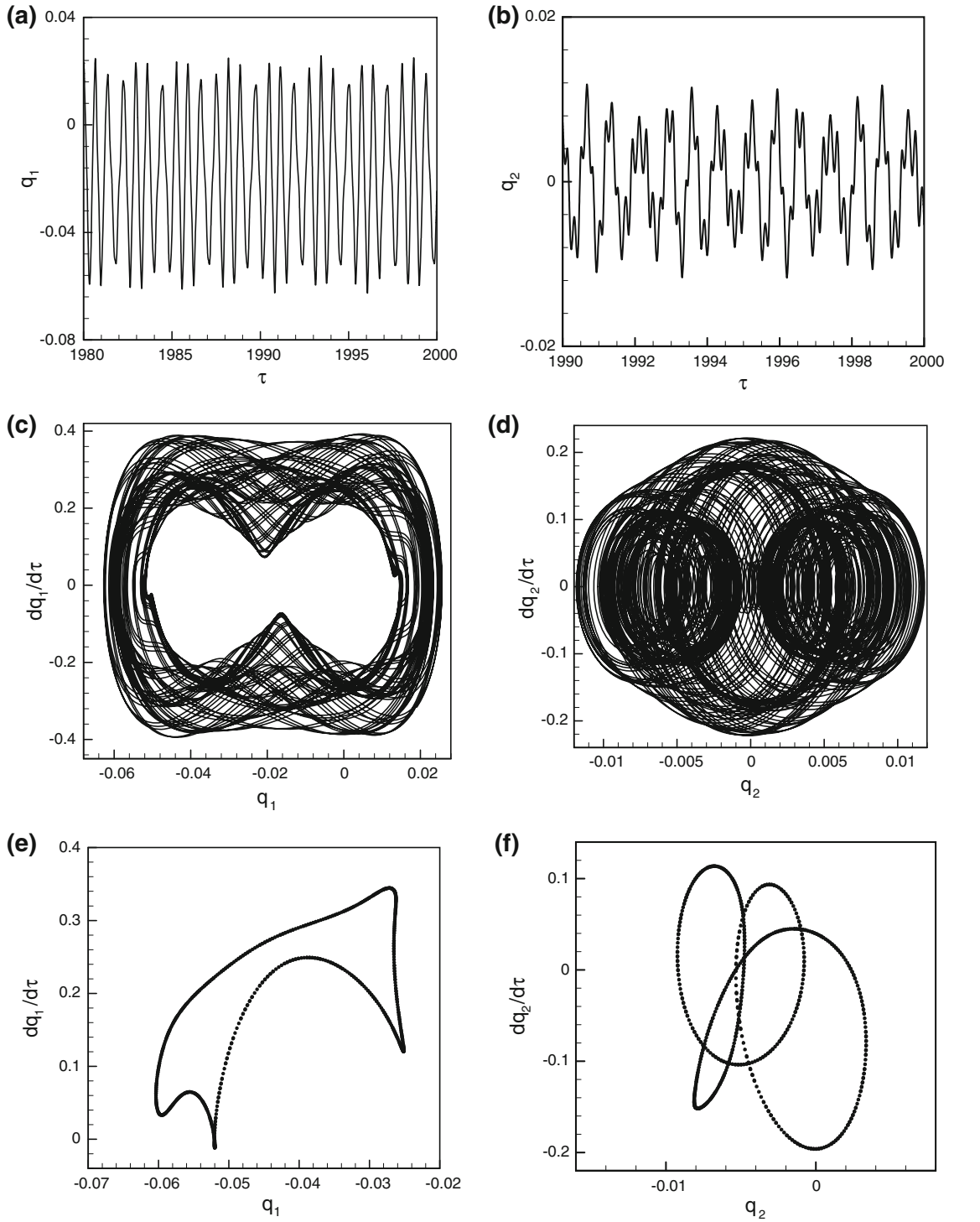


**Fig. 12** Quasiperiodic oscillation for the system of Fig. 10 at $f_1 = 0.70$; **a**, **b** time traces of the $q_1$ and $q_2$ motions, respectively; **c**, **d** phase-plane diagrams of the $q_1$ and $q_2$ motions, respectively; **e**, **f** Poincaré sections of the $q_1$ and $q_2$ motions, respectively

$$\frac{\partial^2\eta}{\partial\tau^2} + 2c\frac{\partial^2\eta}{\partial\xi\partial\tau} + (c^2-1)\frac{\partial^2\eta}{\partial\xi^2} + v_f^2\frac{\partial^4\eta}{\partial\xi^4}$$
$$+v_1^2\frac{\mathrm{d}^2\psi}{\mathrm{d}\xi^2}\int_0^1\frac{\mathrm{d}^2\psi}{\mathrm{d}\xi^2}\eta\mathrm{d}\xi - \frac{v_1^2}{2}\frac{\partial^2\eta}{\partial\xi^2}\int_0^1\left(\frac{\mathrm{d}\psi}{\mathrm{d}\xi}\right)^2\mathrm{d}\xi + \gamma_T\frac{\partial^2\eta}{\partial\xi^2}$$

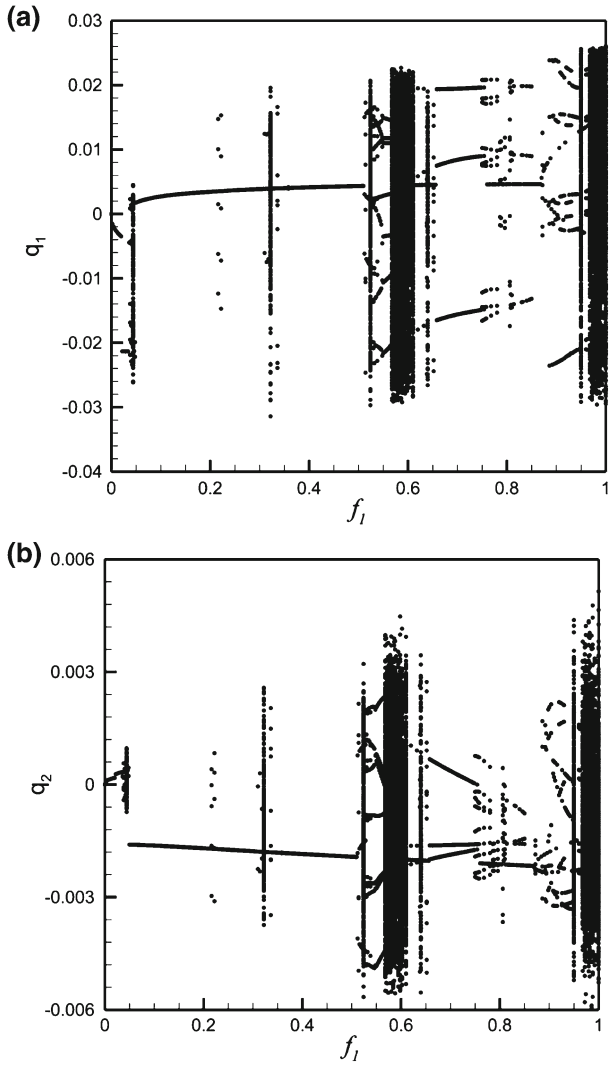


**Fig. 13** Bifurcation diagrams of Poincaré points for increasing forcing amplitude on the system with $\gamma_T = 1.0$, $c = 2.8$, $v_1 = 80$, $v_f = 0.8$, and $\mu = 0.05$; **a** the first mode, and **b** the second mode

$$= \frac{1}{2}v_1^2 \left[ \frac{\mathrm{d}^2\psi}{\mathrm{d}\xi^2} \int_0^1 \left( \frac{\partial \eta}{\partial \xi} \right)^2 \mathrm{d}\xi - 2\frac{\partial^2 \eta}{\partial \xi^2} \int_0^1 \frac{d^2\psi}{\mathrm{d}\xi^2} \eta \mathrm{d}\xi + \frac{\partial^2 \eta}{\partial \xi^2} \int_0^1 \left( \frac{\partial \eta}{\partial \xi} \right)^2 \mathrm{d}\xi \right] + F(\xi)\cos(\Omega\tau). \tag{13}$$

Assuming $F(\xi) = f_1\,\phi_1(\xi)$, and the displacement field in the form of the following series expansion:

$$\eta(\xi, \tau) = \sum_{r=1}^{N} \phi_r(\xi) q_r(\tau), \tag{14}$$

where $\phi_r(x)$ denotes the $r$th hinged-hinged beam eigenfunction and $q_r(\tau)$ represents the $r$th generalized coordinate, and applying the Galerkin method gives $N$ second-order nonlinear ordinary differential equations with coupled terms. These equations are transformed into $2N$ first-order nonlinear ordinary differential equations via change of variables; $N = 10$ is chosen in this paper, i.e., 20 first-order nonlinear ordinary differential equations with coupled terms are considered. The pseudo-arclength continuation technique via AUTO code [60] is used to obtain the frequency response curves about the buckled state. The bifurcation diagrams are obtained

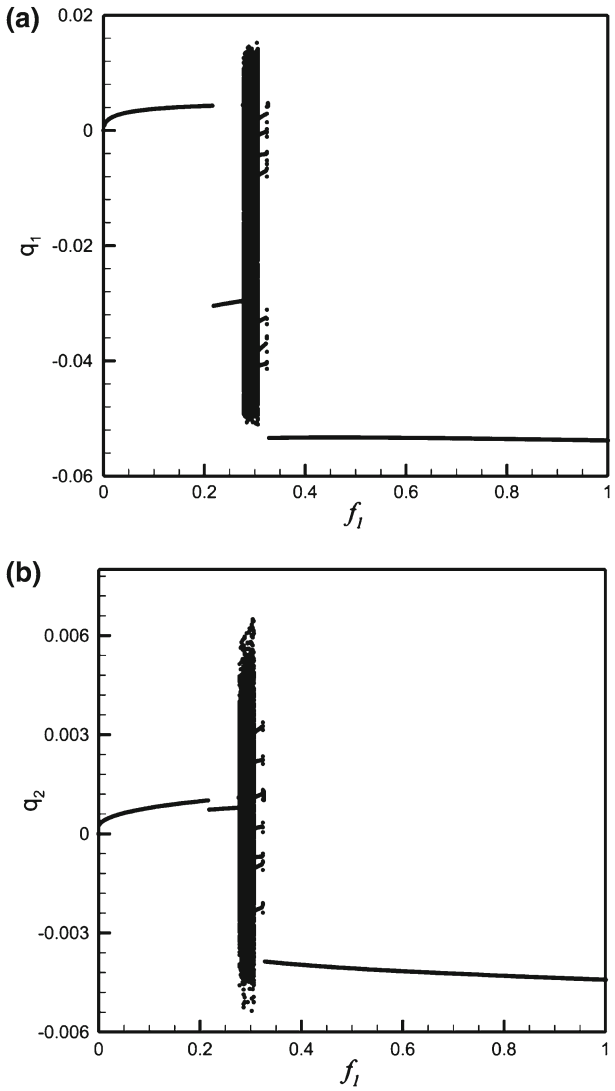


**Fig. 14** Bifurcation diagrams of Poincaré points for increasing forcing amplitude on the system with $\gamma_T = 1.0$, $c = 3.5$, $v_1 = 80$, $v_f = 0.8$, and $\mu = 0.05$; **a** the first mode, and **b** the second mode

by directly integrating the discretized equations through use of a variable step-size Runge–Kutta method. It should also be mentioned that the numerical simulations include dimensionless viscous damping $\mu$.

## 3 Frequency response curves over the buckled state

The frequency response curves of the system are generated in this section using the pseudo-arclength continuation technique for the cases where the system possesses a three-to-one internal resonance between the first two modes and for the case where it is not.

The frequency response curves of the system without internal resonances between the first two modes are shown in Fig. 2a–d. Sub-figure (a, b) shows the maximum and minimum of the first generalized coordinate, respectively, and (c, d) shows the maximum of the oscillation in the second and third modes, respectively. As seen in this figure, the system displays a softening behavior. There are two limit point bifurcations at $\Omega = 0.9914\omega_1$ and $\Omega = 0.9201\omega_1$ and the solution branch between them is unstable. An interesting feature, which is not observed in the frequency response curve of the same system in the subcritical regime, is that the maximum and minimum of the first-mode amplitude are *not* equal; compare sub-figure (a) and (b)—the inward displacement is larger than the outward one.

Carefully selecting system parameters (see the caption of Fig. 3), a three-to-one internal resonance occurs between the first two modes, i.e., the second linear natural frequency of the system is approximately equal to three times the first one. Figure 3a–d shows the frequency response curves of this system. As seen in this figure, again, the maximum and minimum of the first-mode amplitude are not equal. A portion of energy gained from the external excitation by the first mode is transferred to other ones; the outward amplitude of the first mode decreases near the tip of the curve and at the same time the amplitude of the second mode increases. There are five bifurcations in this plot, i.e., four limit points at $\Omega = 0.9772\omega_1$, $\Omega = 0.7113\omega_1$, $\Omega = 0.7118\omega_1$, and $\Omega = 0.7107\omega_1$, and a torus bifurcation at $\Omega = 0.8368\omega_1$.

## 4 Bifurcation diagrams over the buckled state

The global nonlinear dynamics of the system is examined in this section as the forcing amplitude is varied as the bifurcation parameter. This is accomplished using the variable step-size Runge–Kutta method. The computer codes were run for a time interval of [0 2000] dimensionless seconds and the last 30 % of the time trace is taken, which excludes the transient effects. The phase space is sectioned in every period of the external force, which is set to the first linear natural frequency of the system for all cases studied in this section, and the Poincaré maps are plotted versus the forcing amplitude. The step-size is selected 0.002 in the forcing amplitude, and the final state at each step is taken as the initial condition for the next step. It is implied *response* and *amplitude* are with respect to the $q_1$ motion and the amplitude of the $q_1$ motion where it is sectioned, respectively.

The bifurcation diagrams are plotted in Figs. 4 and 10 for $c = 2.8$ and 3.5, respectively, for the case with the thermal factor of $\gamma_T = 0.5$. Increasing the thermal factor to 1.0, from 0.5 in Figs. 4, 10, 13 and 14 are generated.

The bifurcation diagrams of the first two generalized coordinates for an axial speed of $c = 2.8$ are shown in Fig. 4a, b, respectively. As seen in the sub-figure (a), as the forcing amplitude is increased, the system displays initially a periodic oscillation, but soon becomes weakly chaotic in the vicinity of $f_1 = 0.024$. The period is regained at $f_1 = 0.03$ and lasts until the next event. Typical periodic oscillation is illustrated for $f_1 = 0.15$ in Fig. 5 through (a, b) the time histories of the $q_1$ and $q_2$ motions, respectively, (c, d) the phase-plane portraits of the $q_1$ and $q_2$ motions, respectively, and (e, f) the Poincaré maps of the $q_1$ and $q_2$ motions, respectively. In the interval of [0.280 0.362], the motion displays several behavior including periodic, period $-2$, $-3$, $-6$, and $-7$ motions, and chaos. Typical characteristics of the period-7 oscillation for $f_1 = 0.284$ and 0.310 are depicted in Figs. 6 and 7, respectively. As the forcing amplitude is increased even further, different coexisting and strange attractors appear. Two of these attractors at $f_1 = 0.6$ and 0.7 are shown in Figs. 8 and 9, respectively, the first one illustrating a period-5 oscillation and the second one a chaos.

The bifurcation diagram of the same system of Fig. 4, but with higher axial speed (i.e., $c = 3.5$), is shown in Fig. 10. Typical characteristics for $f_1 = 0.430$ and 0.70 are depicted in Figs. 11 and 12, respectively, illustrating two quasiperiodic attractors. Comparing Fig. 10 with 4 shows that it is difficult to draw any conclusion regarding the effect of the axial speed on the bifurcation diagram of the system.

Figures 13 and 14 show the bifurcation diagrams of the same systems of Figs. 4 and 10, respectively, but at a larger thermal factor, i.e., $\gamma_T = 1.0$. These figures reveal that, in general, due to increased thermal factor, many co-existing attractors and higher order bifurcations diminish.

## 5 Conclusions

Thermo-mechanical nonlinear vibrations and stability of a buckled axially moving beam have been investigated by means of the pseudo-arclength continuation technique which is appropriate for continuation and bifurcation analysis of the system near resonance, as well as via direct-time integration suitable for constructing the bifurcation diagrams. Dynamical characteristics of the system have been presented in the form of time traces, phase-plane portraits, Poincaré sections, frequency response curves, and bifurcation diagrams. The near-resonance response of the system is a softening-type with limit point and torus bifurcations. The results for the global dynamics of the system over the buckled state showed that, depending on different system parameters, very rich nonlinear dynamics involving periodic, quasiperiodic, period-$n$, and chaotic oscillations is displayed by the system. This work can be extended considering both longitudinal and transverse displacements. Moreover, the case of time-dependent axial speed can be of interest.

## References


1. Swope, R.D., Ames, W.F.: Vibrations of a moving threadline. J. Frank. Inst. **275**, 36–55 (1963)
2. Mote, C.D.J.: Dynamic stability of axially moving materials. Shock Vib. Dig. **4**(4), 2–11 (1972)
3. Thurman, A.L., Mote, C.D.J.: Free, periodic, nonlinear oscillation of an axially moving strip. ASME J. Appl. Mech. **36**, 83–91 (1969)
4. Shih, L.Y.: Three-dimensional non-linear vibration of a traveling string. Int. J. Non-Linear Mech. **6**, 427–434 (1971)
5. Yuh, J., Young, T.: Dynamic modeling of an axially moving beam in rotation: simulation and experiment. J. Dyn. Syst. Meas. Control **113**, 34–40 (1991)
6. Treyssède, F.: Prebending effects upon the vibrational modes of thermally prestressed planar beams. J. Sound Vib. **307**, 295–311 (2007)
7. Pradeep, V., Ganesan, N., Bhaskar, K.: Vibration and thermal buckling of composite sandwich beams with viscoelastic core. Compos. Struct. **81**, 60–69 (2007)
8. Sharnappa, G.N., Sethuraman, R.: Dynamic modeling of active constrained layer damping of composite beam under thermal environment. J. Sound Vib. **305**, 728–749 (2007)
9. Xiang, H.J., Yang, J.: Free and forced vibration of a laminated FGM Timoshenko beam of variable thickness under heat conduction. Compos. B Eng. **39**, 292–303 (2008)
10. Wu, G.: The analysis of dynamic instability and vibration motions of a pinned beam with transverse magnetic fields and thermal loads. J. Sound Vib. **284**, 343–360 (2005)
11. Manoach, E., Ribeiro, P.: Coupled, thermoelastic, large amplitude vibrations of Timoshenko beams. Int. J. Mech. Sci. **46**, 1589–1606 (2004)
12. Ghayesh, M.H., Kazemirad, S., Darabi, M.A., Woo, P.: Thermo-mechanical nonlinear vibration analysis of a spring-mass-beam system. Arch. Appl. Mech. **82**, 317–331 (2012)
13. Chen, L.-Q.: Analysis and control of transverse vibrations of axially moving strings. Appl. Mech. Rev. **58**, 91–116 (2005)
14. Mote, J.C.D.: On the nonlinear oscillation of an axially moving string. ASME J. Appl. Mech. **33**, 463–464 (1966)
15. Pakdemirli, M., Ulsoy, A.G., Ceranoglu, A.: Transverse vibration of an axially accelerating string. J. Sound Vib. **169**, 179–196 (1994)
16. Pakdemirli, M., Ulsoy, A.G.: Stability analysis of an axially accelerating string. J. Sound Vib. **203**, 815–832 (1997)
17. Öz, H.R., Pakdemirli, M., Özkaya, E.: Transition behaviour from string to beam for an axially accelerating material. J. Sound Vib. **215**, 571–576 (1998)
18. Pakdemirli, M., Özkaya, E.: Approximate boundary layer solution of a moving beam problem. Math. Comput. Appl. **3**, 93–100 (1998)
19. Öz, H.R., Pakdemirli, M.: Vibrations of an axially moving beam with time-dependent velocity. J. Sound Vib. **227**, 239–257 (1999)
20. ÖZkaya, E., Pakdemirli, M.: Vibrations of an axially accelerating beam with small flexural stiffness. J. Sound Vib. **234**, 521–535 (2000)
21. Öz, H.R., Pakdemirli, M., Boyaci, H.: Non-linear vibrations and stability of an axially moving beam with time-dependent velocity. Int. J. Non-Linear Mech. **36**, 107–115 (2001)
22. Yang, X.-D., Tang, Y.-Q., Chen, L.-Q., Lim, C.W.: Dynamic stability of axially accelerating Timoshenko beam: Averaging method. Eur. J. Mech. A Solids **29**, 81–90 (2010)
23. Chen, L.-Q., Tang, Y.-Q., Lim, C.W.: Dynamic stability in parametric resonance of axially accelerating viscoelastic Timoshenko beams. J. Sound Vib. **329**, 547–565 (2010)
24. Ding, H., Chen, L.-Q.: Galerkin methods for natural frequencies of high-speed axially moving beams. J. Sound Vib. **329**, 3484–3494 (2010)
25. Chen, L.H., Zhang, W., Yang, F.H.: Nonlinear dynamics of higher-dimensional system for an axially accelerating viscoelastic beam with in-plane and out-of-plane vibrations. J. Sound Vib. **329**, 5321–5345 (2010)
26. Chen, L.-Q., Chen, H.: Asymptotic analysis on nonlinear vibration of axially accelerating viscoelastic strings with the standard linear solid model. J. Eng. Math. **67**, 205–218 (2010)
27. Chen, L.-Q., Ding, H.: Steady-State transverse response in coupled planar vibration of axially moving viscoelastic beams. J. Vib. Acoust. **132**, 011009 (2010)
28. Ding, H., Zhang, G.C., Chen, L.-Q.: Supercritical equilibrium solutions of axially moving beams with hybrid boundary conditions. Mech. Res. Commun. **38**, 52–56 (2011)
29. Marynowski, K., Kapitaniak, T.: Kelvin-Voigt versus Bürgers internal damping in modeling of axially moving viscoelastic web. Int. J. Non-Linear Mech. **37**, 1147–1161 (2002)
30. Marynowski, K.: Non-linear vibrations of an axially moving viscoelastic web with time-dependent tension. Chaos Solit. Fract. **21**, 481–490 (2004)
31. Marynowski, K., Kapitaniak, T.: Zener internal damping in modelling of axially moving viscoelastic beam with time-dependent tension. Int. J. Non-Linear Mech. **42**, 118–131 (2007)
32. Suweken, G., Van Horssen, W.T.: On the weakly nonlinear, transversal vibrations of a conveyor belt with a low and time-varying velocity. Nonlinear Dyn. **31**, 197–223 (2003)
33. Suweken, G., Van Horssen, W.T.: On the transversal vibrations of a conveyor belt with a low and time-varying velocity. Part II: the beam-like case. J. Sound Vib. **267**, 1007–1027 (2003)
34. Suweken, G., Van Horssen, W.T.: On the transversal vibrations of a conveyor belt with a low and time-varying velocity. Part I: the string-like case. J. Sound Vib. **264**, 117–133 (2003)
35. Sze, K.Y., Chen, S.H., Huang, J.L.: The incremental harmonic balance method for nonlinear vibration of axially moving beams. J. Sound Vib. **281**, 611–626 (2005)
36. Huang, J.L., Su, R.K.L., Li, W.H., Chen, S.H.: Stability and bifurcation of an axially moving beam tuned to three-to-one internal resonances. J. Sound Vib. **330**, 471–485 (2011)

37. Stylianou, M., Tabarrok, B.: Finite element analysis of an axially moving beam, part I: time integration. J. Sound Vib. **178**, 433–453 (1994)
38. Riedel, C.H., Tan, C.A.: Coupled, forced response of an axially moving strip with internal resonance. Int. J. Non-Linear Mech. **37**, 101–116 (2002)
39. Hwang, S.J., Perkins, N.C.: Supercritical stability of an axially moving beam part II: vibration and stability analyses. J. Sound Vib. **154**, 397–409 (1992)
40. Tan, C.A., Yang, B., Mote, J.C.D.: Dynamic response of an axially moving beam coupled to hydrodynamic bearings. J. Vib. Acoust. **115**, 9–15 (1993)
41. Pellicano, F., Zirilli, F.: Boundary layers and non-linear vibrations in an axially moving beam. Int. J. Non-Linear Mech. **33**, 691–711 (1998)
42. Ghayesh, M.H., Balar, S.: Non-linear parametric vibration and stability of axially moving visco-elastic Rayleigh beams. Int. J. Solids Struct. **45**, 6451–6467 (2008)
43. Ghayesh, M.H.: Nonlinear transversal vibration and stability of an axially moving viscoelastic string supported by a partial viscoelastic guide. J. Sound Vib. **314**, 757–774 (2008)
44. Ghayesh, M.H.: Stability characteristics of an axially accelerating string supported by an elastic foundation. Mech. Mach. Theory **44**, 1964–1979 (2009)
45. Ghayesh, M.H., Yourdkhani, M., Balar, S., Reid, T.: Vibrations and stability of axially traveling laminated beams. Appl. Math. Comput. **217**, 545–556 (2010)
46. Ghayesh, M.H.: Parametric vibrations and stability of an axially accelerating string guided by a non-linear elastic foundation. Int. J. Non-Linear Mech. **45**, 382–394 (2010)
47. Ghayesh, M.H., Païdoussis, M.P.: Three-dimensional dynamics of a cantilevered pipe conveying fluid, additionally supported by an intermediate spring array. Int. J. Non-Linear Mech. **45**, 507–524 (2010)
48. Ghayesh, M.H., Païdoussis, M.P.: Dynamics of a fluid-conveying cantilevered pipe with intermediate spring support. ASME Conf. Proc. (FEDSM 2010) 893–902 (2010)
49. Ghayesh, M.H., Balar, S.: Non-linear parametric vibration and stability analysis for two dynamic models of axially moving Timoshenko beams. Appl. Math. Model. **34**, 2850–2859 (2010)
50. Sahebkar, S.M., Ghazavi, M.R., Khadem, S.E., Ghayesh, M.H.: Nonlinear vibration analysis of an axially moving drillstring system with time dependent axial load and axial velocity in inclined well. Mech. Mach. Theory **46**, 743–760 (2011)
51. Ghayesh, M.H., Païdoussis, M.P., Modarres-Sadeghi, Y.: Three-dimensional dynamics of a fluid-conveying cantilevered pipe fitted with an additional spring-support and an end-mass. J. Sound Vib. **330**, 2869–2899 (2011)
52. Ghayesh, M.H., Moradian, N.: Nonlinear dynamic response of axially moving, stretched viscoelastic strings. Arch. Appl. Mech. **81**, 781–799 (2011)
53. Ghayesh, M.H.: Stability and bifurcations of an axially moving beam with an intermediate spring support. Nonlinear Dyn. (2011, in press)
54. Ghayesh, M.H.: On the natural frequencies, complex mode functions, and critical speeds of axially traveling laminated beams: parametric study. Acta Mech. Solida Sin. **24**, 373–382 (2011)
55. Ghayesh, M.H.: Nonlinear forced dynamics of an axially moving viscoelastic beam with an internal resonance. Int. J. Mech. Sci. **53**, 1022–1037 (2011)
56. Ghayesh, M.H., Kafiabad, H.A., Reid, T.: Sub- and super-critical nonlinear dynamics of a harmonically excited axially moving beam. Int. J. Solids Struct. **49**, 227–243 (2012)
57. Ghayesh, M.H., Kazemirad, S., Amabili, M.: Coupled longitudinal-transverse dynamics of an axially moving beam with an internal resonance. Mech. Mach. Theory **52**, 18–34 (2012)
58. Ghayesh, M.H.: Subharmonic dynamics of an axially accelerating beam. Arch. Appl. Mech. accepted (2012)
59. Pellicano, F., Vestroni, F.: Nonlinear dynamics and bifurcations of an axially moving beam. J. Vib. Acoust. **122**, 21–30 (2000)
60. Doedel, E.J., Champneys, A.R., Fairgrieve, T.F., Kuznetsov, Y.A., Sandstede, B., Wang, X.: AUTO 97: Continuation and Bifurcation Software for Ordinary Differential Equations (with HomCont). Concordia University, Montreal (1998)